Article

Current Biology

A Class of Visual Neurons with Wide-Field Properties Is Required for Local Motion Detection

Graphical Abstract

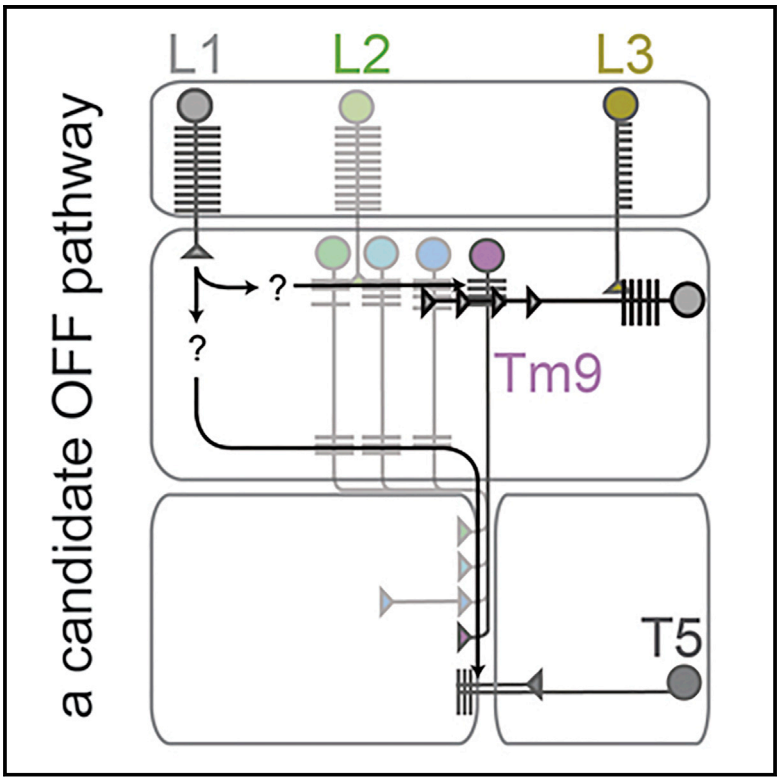

Authors

Yvette E. Fisher, Jonathan C.S. Leong, Katja Sporar, Madhura D. Ketkar, Daryl M. Gohl, Thomas R. Clandinin, Marion Silies

Correspondence

m.silies@eni-g.de

In Brief

The extraction of motion signals requires a nervous system to compare signals over space and time. Fisher et al. identify a visual pathway that has large receptive fields and shows sustained responses to contrast. Thus, it cannot provide the local information needed to extract motion signals but is still required for direction-selective outputs.

Highlights

- Forward genetics identifies the behaviorally critical visual neuron Tm9
- Tm9 shows sustained responses and integrates both L3 and L1 inputs
- Despite its columnar anatomy, Tm9 has large spatial receptive fields
- Tm9 is widely required for responses of the direction-selective T5 neurons

Fisher et al., 2015, Current Biology *25*, 3178–3189
December 21, 2015
http://dx.doi.org/10.1016/j.cub.2015.11.018

CellPress

CellPress

Current Biology
Article

A Class of Visual Neurons with Wide-Field Properties Is Required for Local Motion Detection

Yvette E. Fisher,[1,3] Jonathan C.S. Leong,[1,3] Katja Sporar,[2] Madhura D. Ketkar,[2] Daryl M. Gohl,[1,4] Thomas R. Clandinin,[1] and Marion Silies[2,*]

[1]Department of Neurobiology, Stanford University, Stanford, CA 94305, USA
[2]European Neuroscience Institute, Grisebachstrasse 5, 37077 Göttingen, Germany
[3]Co-first author
[4]Present address: University of Minnesota Genomics Center, Minneapolis, MN 55455, USA
*Correspondence: m.silies@eni-g.de
http://dx.doi.org/10.1016/j.cub.2015.11.018

SUMMARY

Visual motion cues are used by many animals to guide navigation across a wide range of environments. Long-standing theoretical models have made predictions about the computations that compare light signals across space and time to detect motion. Using connectomic and physiological approaches, candidate circuits that can implement various algorithmic steps have been proposed in the *Drosophila* visual system. These pathways connect photoreceptors, via interneurons in the lamina and the medulla, to direction-selective cells in the lobula and lobula plate. However, the functional architecture of these circuits remains incompletely understood. Here, we use a forward genetic approach to identify the medulla neuron Tm9 as critical for motion-evoked behavioral responses. Using in vivo calcium imaging combined with genetic silencing, we place Tm9 within motion-detecting circuitry. Tm9 receives functional inputs from the lamina neurons L3 and, unexpectedly, L1 and passes information onto the direction-selective T5 neuron. Whereas the morphology of Tm9 suggested that this cell would inform circuits about local points in space, we found that the Tm9 spatial receptive field is large. Thus, this circuit informs elementary motion detectors about a wide region of the visual scene. In addition, Tm9 exhibits sustained responses that provide a tonic signal about incoming light patterns. Silencing Tm9 dramatically reduces the response amplitude of T5 neurons under a broad range of different motion conditions. Thus, our data demonstrate that sustained and wide-field signals are essential for elementary motion processing.

INTRODUCTION

Visual motion cues drive robust, innate behavioral responses in many animals and are used to navigate, find food, or escape predators. Motion information is initially computed from visual inputs by discrete circuits, elementary motion detectors (EMDs), which measure motion signals in small regions of retinotopic space. To extract motion information, each EMD has to sample light signals from adjacent points in space and compare them across time, performing a paradigmatic neural computation. Here, we identify a neuron that is essential for motion—guided behaviors that contributes to motion detection by providing tonic information about large regions of visual space that is directly incorporated into EMDs.

The algorithmic basis of motion detection has been studied in a variety of experimental systems, creating an excellent context in which to dissect the circuit implementation of neural computation [1, 2]. In insects, the Hassenstein Reichardt correlator (HRC) model predicts a wealth of behavioral and physiological data. This EMD model correlates signals that arise from two neighboring points in space, after one input has been temporally delayed compared to the other [3–5]. By rectifying contrast inputs into increment and decrement components, and splitting the motion computation into different combinations of ON and OFF signals, it is possible to construct motion detectors that selectively respond to moving light and dark edges [3].

Recent years have seen considerable progress toward identifying the circuits and organizational principles that govern the extraction of elementary motion cues in *Drosophila*. In the fly visual system, the extraction of motion cues is segregated, both behaviorally and physiologically, into two pathways, which are selective for either moving ON or OFF edges [6, 7]. This segregation emerges immediately postsynaptic to photoreceptors where the lamina neuron L1 provides retinotopic inputs to the ON pathway and the lamina neuron L2 provides the major input to the OFF pathway [6, 7] (Figures 1A and 1B). Whereas L1 and L2 respond to light independent of motion, downstream computations that take place in the medulla and the lobula transform these signals into direction-selective responses observed within T4 and T5 neurons [11, 12]. Both T4 and T5 exist in four subtypes, each of which responds to one of the cardinal directions of motion. Whereas T4 is specialized for moving ON edges, T5 responds selectively to moving OFF edges [11]. Importantly, simultaneous genetic silencing of combinations of ON or OFF pathway neurons either at the inputs or the output level leads to strong behavioral deficits in motion detection [7, 13, 14]. Anatomical studies using serial electron

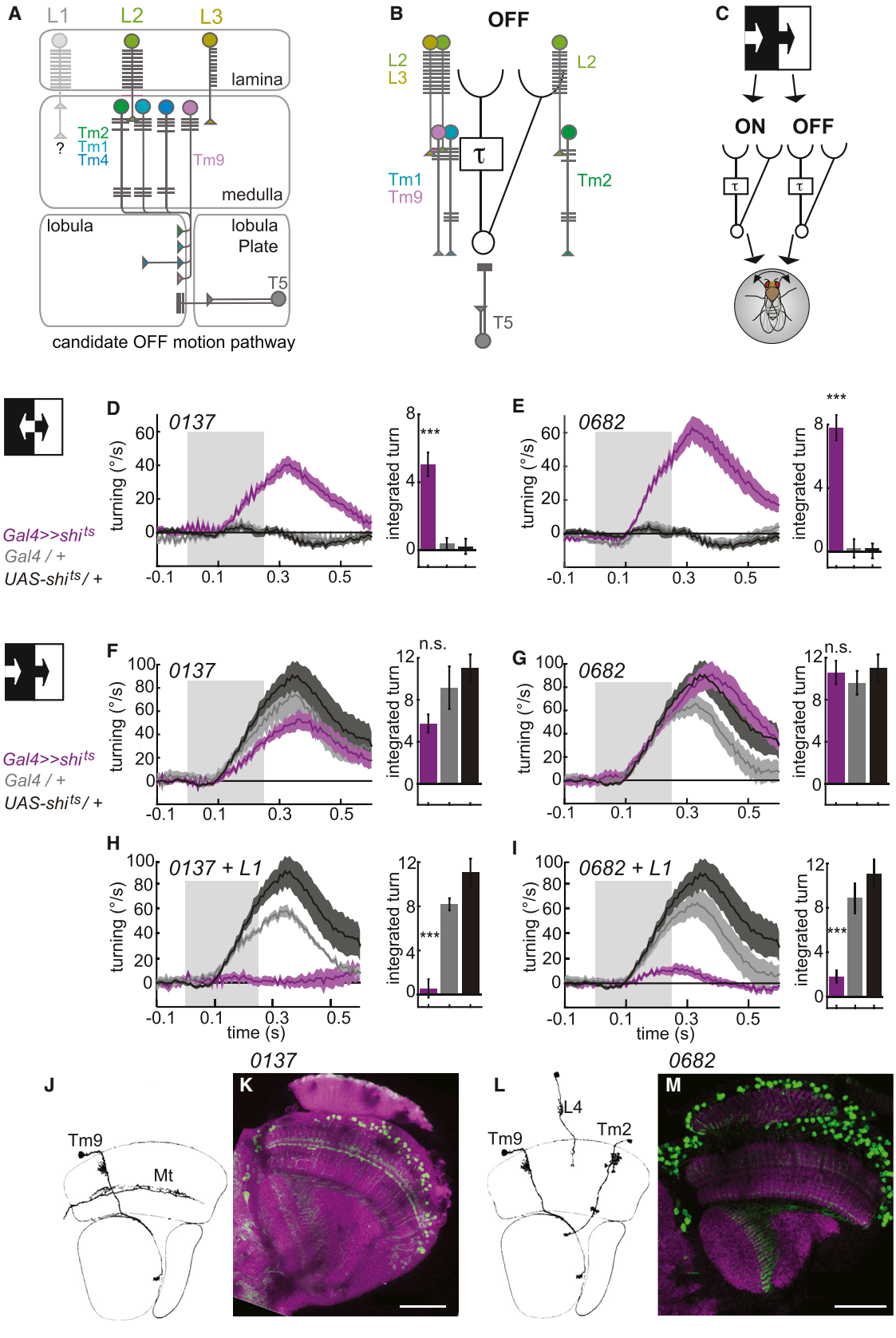

(legend on next page)

microscopy (EM) have mapped the main synaptic connections between L1 and T4, identifying the medulla intrinsic neuron Mi1 and the transmedullary neuron Tm3 for the ON pathways, whereas Tm1 and Tm2 neurons are the strongest links between L2 and T5 in the OFF pathway [8, 15] (Figures 1A and 1B). These four medulla neuron types display physiological properties that map onto computational predictions, including temporal delays and signal rectification [9, 16] (Figure 1B). However, additional data obtained from EM studies and behavioral studies indicate that EMD circuits are more complex than this favored pattern of connectivity would suggest [15]. Sixty different cell types have been identified in the medulla [10, 17], suggesting that coding could be more distributed. In support of this notion, even at the level of the lamina, L2 is not the only input channel for motion responses to OFF edges, but rather additional contributions are required from L3 and L1 [13] (Figure 1A). Also, other candidate neurons such as Tm4 and Tm9 have been proposed to play roles in OFF motion detection as they make a large number of output synapses onto T5 dendrites in the lobula [8, 15] (Figures 1A and 1B). Thus, additional circuit components may also play functionally important roles in motion detection. Because EMDs can produce directional signals from only local cues [4, 12, 18], they are not predicted to incorporate information from across a wide region of space and time. However, given the versatility and robustness of motion-guided behaviors, combined with the neuronal diversity in the medulla, it seems plausible that motion-detecting circuits might incorporate additional information from the visual scene.

Here, we used two independent genetic approaches to identify visual interneurons that are necessary for behavioral responses to moving OFF edges. We identified a transmedullary neuron, Tm9, whose physiological properties do not map onto classical EMD models but which is required for EMD function. In particular, this neuron carries wide-field information over long timescales and integrates ON and OFF pathway inputs. We show that Tm9 provides critical input to OFF edge motion detection across a wide range of conditions. Thus, we identify and characterize a behaviorally relevant circuit that is a central component of elementary motion detection.

RESULTS

Forward Genetics Identifies Neurons that Are Required for Motion-Guided Behavior

We first sought to identify behaviorally critical components of motion-detecting circuits. Given that the OFF pathway utilizes a combination of inputs, making functional specializations in downstream circuits likely, we focused on identifying medulla circuit components in this pathway. Both ON and OFF edges contribute to behavioral responses to motion (Figure 1C), and only blocking both pathways simultaneously results in motion blindness to rotational stimuli [7, 13, 19]. To circumvent this inherent circuit redundancy, we employed two parallel forward genetic approaches to identify novel neurons that contribute to the detection of moving dark edges.

In a first approach, we blocked neural activity in a set of 57 InSITE enhancer trap Gal4 lines that had expression in the medulla while simultaneously silencing L1 through expression of *UAS-shibire^{ts}* (*UAS-shi^{ts}*), a temperature-inducible blocker of synaptic activity [20]. Using a population-based behavioral assay (described in [13, 21]), we identified that the line *0682-Gal4* dramatically enhanced the L1 phenotype, suggesting that this driver line is expressed in OFF pathway neurons (data not shown).

In a second approach, we used a single fly behavioral assay in which a fly walks on an air-cushioned ball surrounded by visual displays, allowing us to precisely control the visual presentation while monitoring the animal's behavioral response (Figure 1C). Given the contribution of both ON and OFF pathways to motion, we chose a stimulus in which rotating ON and OFF edges moved in opposite direction, the ''opposing edges'' stimulus [7]. Control flies with intact motion processing circuits that respond to both edge types show very little net turning as the outputs of the two pathways cancel each other (Figures 1D and 1E). Conversely, when circuit components that differentially affect one of the two pathways are disrupted, flies turn in the direction predicted by the motion signal from the intact pathway [7, 11, 13]. Flies appeared more motivated to move in this assay compared to the population assay. Thus, we first tested Gal4 lines with prominent expression in the medulla that did not walk well in the population assay. From this collection, we

Figure 1. Forward Genetic Screens Identify Neurons of the OFF Pathway

(A) Schematic of the *Drosophila* visual system. Candidate elements of the OFF-T5 pathway are shown. Circles represent cell bodies, bars are dendrites, and triangles are synaptic terminals. Candidate medulla interneurons have been identified downstream of L2 and L3; the pathway by which L1 contributes to OFF edge detection was unknown (denoted by a "?").

(B) A simplified model of the HRC and its candidate circuits in the OFF pathway. Tm2 has faster temporal dynamics than Tm1, and spatial offsets in wiring onto T5 enables sampling of adjacent points in space as Tm2 inputs are offset compared to both Tm1 and Tm9 [8, 9].

(C) ON and OFF pathways are separated yet together guide behavioral responses to motion.

(D–I) Turning responses that were obtained using a single fly behavioral assay in which a tethered fly walks on an air-cushioned ball. Flies see motion stimuli in which moving ON and OFF edges are rotating around the fly and move either in opposite directions (''opposing edges''; D and E) or in the same direction to each other (''rotating grating''; F–I); the gray box shows the 250 ms of stimulus presentation. Each panel shows the experimental *Gal4 >> shi^{ts}* condition (magenta) as well as the corresponding *Gal4/+* (light gray) and *UAS-shi^{ts}/+* (dark gray) controls. The bar plots next to each time trace show integrated responses over a 250 ms window beginning 80 ms after stimulus onset. Shading and error bars denote ±1 SEM. n.s., not significant; ***$p < 0.001$; tested using two-tailed Student's t test against both controls. Sample sizes are n = 6 flies for *UAS-shi^{ts}/+*, n = 9 for *0137/+*, n = 7 for *0137>>shi^{ts}*, n = 8 for *0682/+*, and n = 9 for *0682>>shi^{ts}* in (D)–(G). Sample sizes are n = 6 flies for *UAS-shi^{ts}/+*, n = 6 for *L1^{c202a}-Gal4+0137/+*, n = 6 for *L1^{c202a}-Gal4+0137>>shi^{ts}*, n = 9 for *L1^{c202a}-Gal4+0682/+*, and n = 9 for *L1^{c202a}-Gal4+0682>>shi^{ts}* in (H) and (I).

(J–M) Characterization of the *0137-Gal4* and *0682-Gal4* expression patterns. (K and M) Confocal images of adult brains stained with anti-GFP (green) and anti-Bruchpilot (nc82; magenta) are shown. *0137-Gal4* (K) or *0682-Gal4* (M) was driving expression of both *UAS-mCD8::GFP* and *UAS-EGFP*. Scale bars are 50 μm. (J and L) Schematic of the visual system neurons identified in *0137-Gal4* and *0682-Gal4,* adapted from [10].

See also Figure S1.

identified the driver line *0137-Gal4* as having a strong edge-specific phenotype: when tested at the restrictive temperature, *0137-Gal4 UAS-shi^{ts}* flies turned strongly with the direction of moving ON edges of the opposing edges stimulus, whereas control flies did not (Figure 1D). Similarly, the *0682-Gal4* driver line that was initially identified in the population screen showed an indistinguishable phenotype when tested in this single-fly paradigm (Figure 1E). For comparison, we interleaved stimuli in which patterns of ON and OFF edges rotated in the same direction, creating a "rotating grating" stimulus (Figures 1F–1I). Like control flies, both *0137-Gal4 UAS-shi^{ts}* and *0682-Gal4 UAS-shi^{ts}* flies turned in the direction of the rotating grating, following the coordinated movement of ON and OFF edges (Figures 1F and 1G). Thus, these manipulations have specific effects on the detection of OFF edge motion.

The strong preference for moving ON edges in the opposing edge stimulus suggests that neurons targeted in these lines contribute to OFF edge detection. However, this stimulus can only isolate relative, but not absolute, differences in responses to ON and OFF motion. To test whether these neurons were essential to the detection of OFF edges, we measured behavioral responses to the same rotating grating stimulus while abolishing all responses to moving ON edges by silencing L1 and simultaneously blocking neural activity using either *0137-Gal4* or *0682-Gal4*. Strikingly, combinatorial silencing of L1 activity and either the *0137* or the *0682* pattern completely abolished all responses to rotating gratings (Figures 1H and 1I). This effect was as strong as disrupting either the L2 or L3 input channels to motion detection in combination with L1 inputs [7, 13, 19], demonstrating that cell types targeted by *0137-Gal4* and *0682-Gal4* are absolutely required in the OFF pathway for motion-guided behaviors.

Tm9 Is Critical for Moving OFF Edge Detection

We next characterized the *0137-Gal4* and *0682-Gal4* expression patterns to identify the behaviorally relevant neurons targeted by these driver lines. We either expressed GFP in the full Gal4 pattern or stochastically labeled single-cell subsets using a Flp recombinase-based approach [22] (Figures 1J–1M and S1A–S1H). Both lines showed prominent expression in the visual system but also labeled a few cells in the central brain (Figures 1J–1M, S1A, and S1B). In the visual system, *0137*-Gal4 marked two medulla layers (Figures 1J and 1K). Single-cell clones unambiguously identified a neuron type with dendritic arborizations in medulla layers M2/3, an absence of dendrites in the proximal medulla, and a bulb-shaped axon terminal in the first layer of the lobula as the transmedullary neuron Tm9 (Figure S1D) [10]. A single medulla tangential cell with arborizations spanning large areas in the medial medulla was also identified, but the presence of this cell type was variable between individual brains (Figure S1E; data not shown). For the *0682*-Gal4 driver line, expression in the lamina was identified as the neuron L4 with its characteristic proximally restricted dendrites (Figures 1L and 1M). In the medulla, single-cell clones in this line identified a transmedullary neuron with two characteristic dendritic projections in the medial medulla as Tm2 (Figure S1G) and Tm9 (Figures S1G and S1H). To verify that we did not miss any cells using the stochastic labeling approach, we also narrowed down the expression patterns in these driver lines using genetic intersections with *chaGal4-DBD* and *cha-Gal80* (Figures S1I–S1N). These approaches confirmed that *0137-Gal4* was expressed in the medulla neuron Tm9 and a medulla tangential cell, whereas the line *0682-Gal4* was expressed in L4, Tm2, and Tm9 (Figures S1I–S1N). Thus, Tm9 was the only cell type common to these two driver lines. To directly capture this overlap, we reconstituted a split-LexA transcription factor through an intersection of the *0137-p65AD* InSITE swap with *0682-Gal4 UASLexADBD*. As expected from the characterization of the individual expression patterns, expression was only observed in Tm9 (Figure S2A). Tm2 had previously been suggested to function in the OFF pathway, whereas the function of L4 has been controversial [13, 16, 23]. However, the common presence of the transmedullary neuron Tm9 in the two Gal4 lines prompted us to next test the possibility that Tm9 has a critical function in motion detection.

To test the specific requirement of Tm9 in moving OFF edge detection, we used InSITE-mediated replacement of the *0137-Gal4* and generated a *0137-Gal80*. When combined with *0682-Gal4*, *0137-Gal80* efficiently removed Tm9 expression while leaving expression in Tm2 and L4 intact (Figure 2A). Comparing the full *0682-Gal4* expression to the same expression pattern with just Tm9 removed allowed us to examine the behavioral contribution of Tm9. As shown before, silencing of all of the neurons labeled by *0682-Gal4* resulted in the strong preference for rotating ON edges in the opposing edges stimulus (Figures 1E and 2C, dotted gray line). *0682-Gal4*, *0137-Gal80*, *UAS-shi^{ts}*-expressing flies, which lack expression in Tm9, still turned with a significant preference for the direction of rotating ON edges. However, this effect was much weaker than when the full *0682-Gal4* pattern was silenced (Figure 2C). Furthermore, we also blocked activity in L1 together with either *0682-Gal4* or *0682-Gal4*, *0137-Gal80* to test for motion blindness in response to rotating gratings. Strikingly, when Tm9 was removed from the *0682-Gal4* expression pattern, these flies turned normally with the rotating cylinders. Thus, removing Tm9 from the full *0682-Gal4* expression pattern restored the ability of flies to respond to visual motion (Figure 2D). In summary, Tm9, but not Tm2 and L4 neurons, most strongly contributed to moving OFF edge detection.

Finally, we obtained a LexA line with specific expression only in Tm9 in the visual system and very few neurons in the central brain: *Tm9^{R24C08}-LexA* [24] (Figures 2E, 2F, and S2B). Blocking neuronal activity upon expression of a *lexAop-shi^{ts}* transgene under the control of this driver revealed a strong preference for moving ON edges when the opposing edge stimulus was presented (Figure 2G). In addition, simultaneously silencing both L1 and Tm9 by combining the Gal4 and the LexA expression systems abolished all behavioral responses to motion cues (Figure 2H). In summary, these data demonstrate that Tm9 is required for behavioral responses to rotating OFF edges.

OFF Motion Detection Requires Inputs from L1, L3, and Tm9

The OFF pathway utilizes a combination of inputs such that simultaneous silencing of two lamina neurons (L1+L2, L1+L3, or L2+L3) is required to completely abolish behavioral responses to OFF motion [13]. Thus, the complete loss of behavioral responses to motion upon simultaneous silencing of L1 and Tm9 argues that Tm9 could be downstream of L2, L3, or both. To

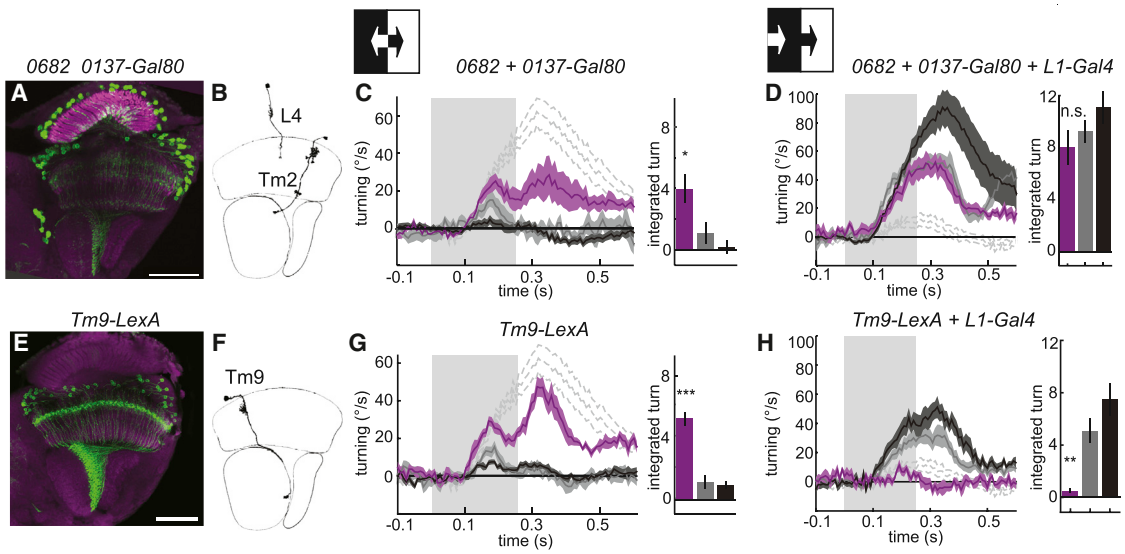

Figure 2. Identification of Behaviorally Relevant Neurons

(A) Confocal image of an adult brain stained with anti-GFP (green) and anti-Bruchpilot (nc82; magenta). *0682-Gal4* combined with suppression by *0137-Gal80* was used to drive both UAS-mCD8::GFP and UAS-EGFP.

(B) Schematic of identified L4 and Tm2 neurons for comparison, adapted from [10].

(C and D) Turning behavior in response to rotational stimuli: opposing edges (C) and rotating gratings (D). Each panel shows the experimental *Gal4 >> shi^{ts}* condition (magenta) as well as the corresponding driver line control *Gal4/+* (light gray) and effector control *UAS-shi^{ts}/+* (dark gray). Grey dotted lines are *0682>>shi^{ts}* in (C), see also Figure 1E, and *L1^{c202a}-Gal4+0682>>shi^{ts}* in (D), see also Figure 1I.

(E) Confocal image of an adult brain stained with anti-GFP (green) and anti-Bruchpilot (nc82; magenta). *Tm9-LexA* was driving lexAop-CD8::GFP. Scale bars are 50 μm in (A) and (E).

(F) Schematic of Tm9 neuron for comparison, adapted from [10].

(G and H) Turning behavior in response to rotational stimuli: opposing edges (G) and rotating gratings (H). Each panel shows the experimental *LexA >> shi^{ts}* or *LexA* and *Gal4 >> shi^{ts}* condition (magenta) as well as the corresponding driver line control *LexA/+* or *LexA/+* and *Gal4/+* (light gray) and effector control *lexAop-shi^{ts}/+* or *lexAop-shi^{ts}/+* and *UAS-shi^{ts}/+* (dark gray). Grey dotted lines are *0682>>shi^{ts}* in (G), see also Figure 1E, and *L1^{c202a}-Gal4+0682>>shi^{ts}* in (H), see also Figure 1I. The bar plots next to each time trace show integrated responses over a 250-ms window beginning 80 ms after stimulus onset. Shading and error bars denote ±1 SEM. *p < 0.05; **p < 0.01; ***p < 0.001; tested using two-tailed Student's t test against both controls. Sample sizes are n = 6 flies for *UAS-shi^{ts}/+*, n = 6 for *0682+0137-Gal80/+*, n = 7 for *0682+0137-Gal80>>shi^{ts}*, n = 9 for *L1^{c202a}-Gal4+0682-Gal4+0137-Gal80/+*, and n = 9 for *L1^{c202a}-Gal4+0682-Gal4+0137-Gal80>>shi^{ts}* in (C) and (D). Sample sizes are n = 9 flies for *lexAop-shi^{ts}/+*, n = 8 for *Tm9-LexA /+*, n = 6 for *Tm9-LexA >> lexAop-shi^{ts}*, n = 9 for *lexAop-shi^{ts}+UAS-shi^{ts}/+*, n = 10 *for Tm9-LexA + L1 ^{c202a}-Gal4/+*, and n = 5 for *L1^{c202a}-Gal4+ Tm9-LexA >> lexAop-shi^{ts} + UAS-shi^{ts}* in (G) and (H). See also Figure S2.

distinguish these possibilities, we probed genetic interactions between Tm9 and lamina neurons while measuring behavioral responses to moving OFF edges. To do this, we used the *0137-Gal4* driver line. Silencing *0137-Gal4* neurons alone led only to a very modest reduction in behavioral responses to moving OFF edges (Figure S2C), a phenotype that was not enhanced by simultaneously silencing L3 in this background (Figure S2D). By contrast, simultaneous silencing of *0137-Gal4* and either L1 or L2 completely abolished turning responses to rotating OFF edges (Figures S2E and S2F). These interactions are identical to silencing L3 in combination with either L1 or L2 and strongly argue that Tm9 receives functional inputs from L3. These data provide additional support for a role of L1 in OFF edge detection, as previously proposed [13]. Finally, silencing *0137-Gal4* alone does not lead to a deficit in ON edge detection, and silencing *0137-Gal4* in combination with L1, L2, or L3 does not enhance the phenotype produced by silencing the individual lamina neurons (Figures S2G–S2J).

Tm9 Responses Require Inputs from Both L3 and L1

We next characterized physiological properties of Tm9 using in vivo two-photon calcium imaging in which the genetically encoded calcium indicator GCaMP6f was expressed in Tm9 neurons (Figures 3A and 3B). We recorded calcium signals in single Tm9 axon terminals in the lobula and presented alternating decreases and increases in light intensity filling a screen that was 60° wide in both azimuth and elevation (Figures 3A–3C). In general, calcium signals in Tm9 increased to the offset of light and decreased to the onset of light (Figures 3C, S3A, and S3B). We called this response type "normal" and defined it by a negative correlation with the stimulus polarity. Additionally, a few cells of the opposite response polarity ("inverted responses") were observed at the edges of the lobula region that was responding to the stimulus, consistent with an inhibitory surround (Figures 3C, S3A, and S3B). All of these features are consistent with properties of lamina neuron inputs and would thus be predicted based on excitatory feedforward signaling from these inputs to the OFF motion pathway [9, 13, 16, 25].

Serial EM reconstructions have identified synapses between L3 and Tm9 but have not detected direct synaptic inputs from L1 and L2 [15]. To test the functional relationships between these inputs and Tm9, we imaged calcium responses in Tm9 while silencing the individual lamina neuron types, using independent binary expression systems (Figures 3D–3F). We recorded

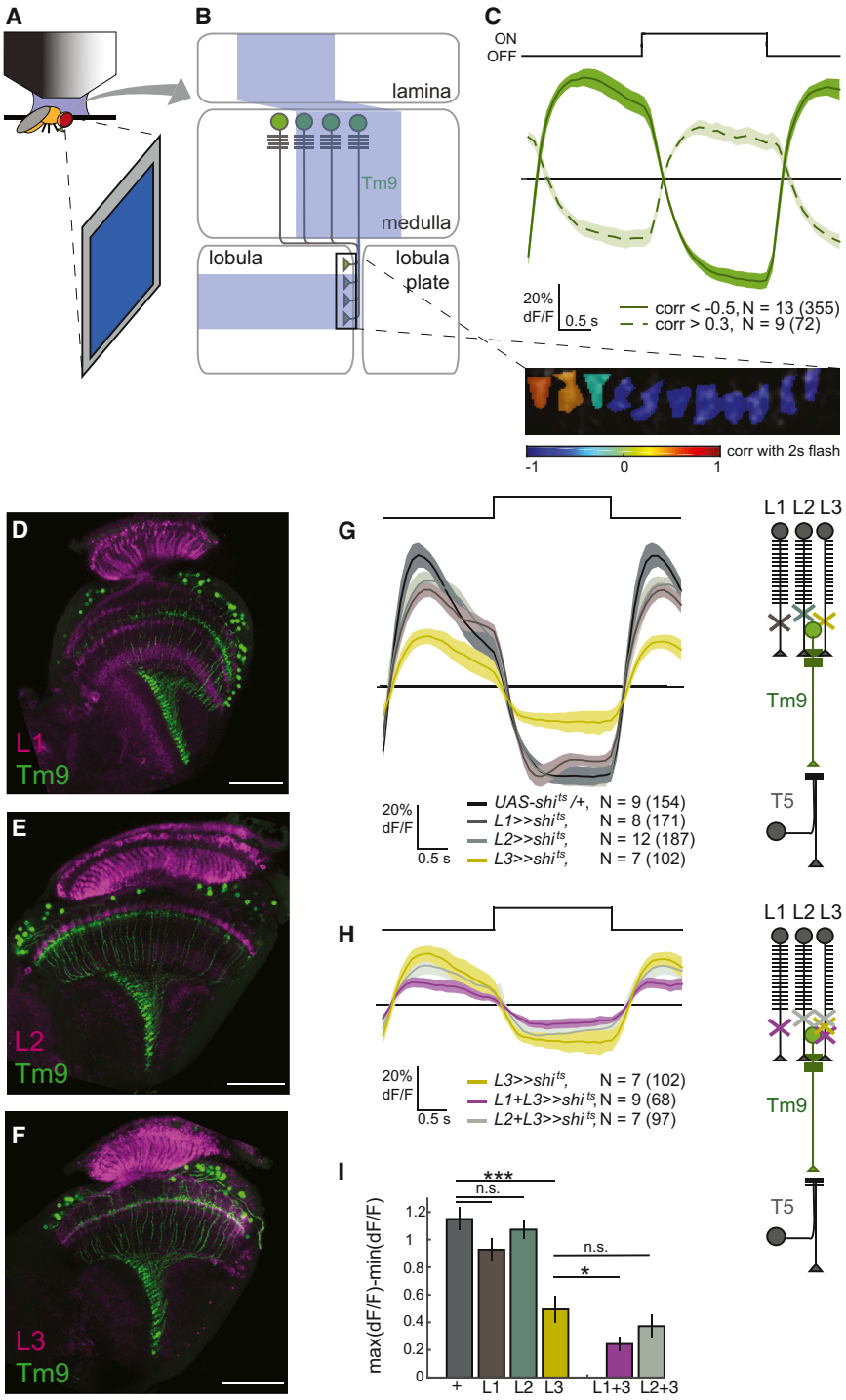

Figure 3. Flash Responses in Tm9 Depend on L3 and L1 Inputs

(A) Schematic of the imaging setup.

(B) Schematic of the visual system. The part of the visual system that is responding to the visual stimulus is highlighted in blue. In the lobula, a typical imaging area is denoted by a rectangle. Due to the retinotopic organization of this brain region, Tm9 terminals were often observed that were within or just outside of the brain region that is directly responding to the stimulus.

(C) (Bottom) Maximum intensity projection of a time series showing GCaMP6f expression in Tm9 terminals in the lobula. Individual terminals that were manually selected are pseudo-colored based on that ROI's cross-correlation with the 2-s full-field flash response to demonstrate how Tm9 "inverted" responses were often observed at the edge of a retinotopic brain region within the imaging frame, consistent with those terminals being "off screen" and thus solely receiving light signals from an inhibitory surround region within their receptive field. (Top) Average calcium responses (ΔF/F) of Tm9 axon terminals to periodic 2-s full-field flashes are shown. Solid lines and dark green shading show responsive cells whose response is negatively correlated (cross-correlation [corr] < −0.5) with the stimulus polarity. These are cells that respond to the stimulus directly. A minority of cells did not respond directly to the stimulus. These inverted responses are positively correlated with the stimulus polarity (dashed lines, light green shading; corr > 0.3). Sample sizes are given as N = no. flies (no. cells).

(D–F) Confocal images of adult brain stained with anti-GFP and anti-dsRed. Tm9LexA was used to drive *lexAop-mCD8::GFP* (green) whereas *L1^{c202a}-Gal4* (D), *L2^{21Dhh}-Gal4* (E), or *L3^{0595}-Gal4* (F) were used to drive *UAS-mCD8::RFP* (magenta). Scale bars are 50 μm.

(G and H) Tm9 responses to full-field flashes were imaged using *Tm9-LexA lexAop-GCaMP6f* whereas either L1, L2, or L3 inputs were synaptically silenced alone or in pairwise combinations. All flies were pre-incubated at 37°C for 1 hr prior to imaging. Shown are average calcium responses (ΔF/F) of Tm9 axon terminals to periodic 2-s full-field flashes.

(I) Bar plot quantifying response magnitude (max-min) of the data shown in (G) and (H). *p < 0.05; ***p < 0.001; tested using unpaired two-tailed Student's t test. Sample sizes are displayed within panel as N = no. flies (no. cells). Shading and error bars denote ±1 SEM.

See also Figure S3.

calcium signals in Tm9 evoked by flashes of light after incubating the flies at the restrictive temperature for Shibire^{ts}. We observed a 57% reduction in the amplitude of normal Tm9 responses upon silencing L3 but no significant reduction when L1 or L2 were silenced individually (Figures 3G and 3I). This confirms that Tm9 requires L3 inputs but also demonstrates that Tm9 must receive at least one additional input signal. Given the known combinatorial interactions in the lamina, we next blocked neural activity in L3 together with silencing either L1 or L2. Interestingly, silencing of L1 and L3 together, but not L2 and L3, significantly reduced the response amplitude of Tm9 neurons to light flashes to 21% of the effector control, or half of the amplitude of L3 silencing alone (Figures 3H and 3I). Thus, L1 provides additional functional inputs to Tm9. We note that the magnitude of this reduction is likely an underestimate, given that our analysis requires a measurable, negatively correlated response from Tm9

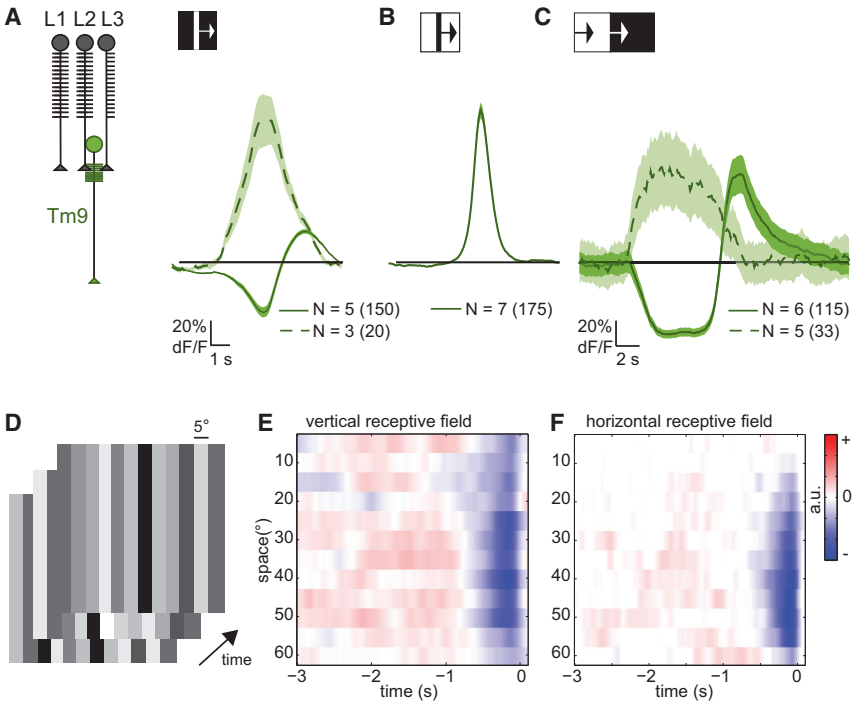

Figure 4. Physiological Response Properties of Tm9 Axon Terminals

(A and B) Averaged aligned response (ΔF/F) of Tm9 axon terminals to an approximately 10°-wide light (A) or dark (B) bar, moving at 20°/s on a background of 100% contrast.

(C) Averaged aligned response (ΔF/F) of Tm9 axon terminals to individual ON and OFF edges, moving at 20°/s. (A–C) Solid and dashed lines correspond to "normal" (corr < −0.5) and inverted responses (corr > 0.1), respectively, as defined by the corr of each individual ROI's response with a 2-s full-field flash stimulus (see also Figure S3). Sample sizes are given as N = no. flies (no. cells). Shading denotes ±1 SEM.

(D) Schematic of a Gaussian white noise stimulus in which twelve 5° wide bars fill the screen and each draw their luminance from a Gaussian distribution.

(E and F) The spatiotemporal receptive fields of two individual Tm9 terminals (from two different flies) obtained using this stimulus, presented either with horizontally oriented bars to map the vertical axis (E) or vertically oriented bars to map the horizontal axis (F) of the receptive fields. Receptive fields were calculated as the fluorescence weighted average stimulus. Red pixels indicate positive correlation with contrast ("+"; increased calcium signal to contrast increments and decreased calcium signal to contrast decrements), and blue pixels indicate negative correlation with contrast ("−"; decreased calcium signal to contrast increments and increased calcium signal to contrast decrements). The color map (a.u.) for each receptive field was scaled to span the full range of contrast values observed per receptive field, while always maintaining the correspondence of white to zero contrast.

See also Figure S4.

cells in order to select signals from normally responding cells. In fact, we only observed visible responses in approximately 25% of the flies in which L1+L3 were silenced (n = 19), compared to 80% for flies in which L2+L3 were silenced and >90% for all other genotypes. Alternatively, the residual response observed when L1+L3 were blocked might also suggest an additional, minor contribution from R8 photoreceptors, as proposed previously [26]. We still observed the inverted response type in all of these genotypes, and blocking activity in individual lamina neuron types or their combinations had similar effects on normal and inverted responses (data not shown).

In summary, these data demonstrate that the L3 pathway provides a major contribution to Tm9. Strikingly, we also identify an unexpected role for L1 in producing Tm9 responses, an effect that likely arises through an intermediate neuron. Taken together with the behavioral data, these imaging studies reinforce a role for both L3 and L1 in OFF edge motion detection.

Tm9 Neurons Respond to Visual Stimuli Across a Wide Visual Field

To further understand how Tm9 contributes to moving OFF edge detection, we next characterized its properties in response to various additional visual stimuli. We first used either light or dark bars that were approximately 10° wide, moving across dark or light backgrounds at 20°/s (Figures 4A and 4B). We observed two types of responses to these moving stimuli that correlated with the polarity of the flash responses described in Figure 3. To extract these motion signals, we separated response types based on the correlation value of an ROI's calcium signal to the flash stimulus (Figures S3A–S3D). Most cells showed a negative correlation with the flash response, consistent with a sign conserving synapse from L3. These cells responded to a moving light bar with first a decrease in their calcium signal, followed by an increase, likely reflecting the bar's movement into and then out of the receptive field center (Figure 4A). Consistent with the inverted response type evoked by light flashes, we also observed that the inverted cells strongly increased their calcium signal to the moving light bar (Figure 4A). When flies were presented with a moving dark bar, all responding cells showed an increase in calcium signal and were negatively correlated with the flash stimulus (the normal response; Figure 4B). Conversely, all cells that had inverted responses to the flash stimulus did not show any responses to the moving dark bar, even if the same ROI responded to the moving light bar (Figures 4A and 4B; data not shown). These data, plus the absence of a biphasic response to moving dark bars, suggest that the surround properties of Tm9 are contrast rectified so as to only convey information about light increments (Figures 4A and 4B). To directly test this prediction, we probed responses to individual moving ON and OFF edges. Consistent with the moving bar responses, calcium signals in Tm9 decreased to the appearing ON edge and increased to the appearing OFF edge (Figure 4C). When compared to previously characterized medulla interneurons [9, 27], Tm9 center responses do not display strong rectification. Interestingly, cells with inverted responses, which primarily receive surround input, only increased their calcium signal to the moving ON edge, but not the OFF edge, confirming that the inhibitory surround is contrast rectified (Figure 4C). Finally, no difference in response

strength was observed to motion in any of the eight directions (Figure S3E).

Interestingly, many of the responses evoked by the moving bar stimuli lasted longer than expected from the speed and width of the bar. These prolonged responses raised the possibility that the receptive field of Tm9 is larger than predicted by the columnar anatomy of the cell. To directly measure the spatial extent of Tm9 responses, we mapped Tm9 receptive fields with a Gaussian noise stimulus that probed both space and time (Figure 4D). We displayed frames that comprised 12 bars, with each bar subtending 5° in either elevation or azimuth, where the intensity of each bar was changed over time according to a Gaussian distribution (see Experimental Procedures). Most of the spatiotemporal receptive fields that we extracted showed a strong inverse correlation between the calcium response and the contrast polarity of the stimulus, consistent with our previous measurements using flash stimuli (Figures 3C, 4E, 4F, S4A, and S4B). These receptive fields reveal that Tm9 responses were driven strongly by stimuli closely preceding the response, peaking at approximately 200 ms. A weaker phase of the opposite polarity extended further back in time (Figures 4E, 4F, S4A, and S4B). These receptive fields were also very large, often spanning the full 60° extent of the screen used in our apparatus (Figures 4E, 4F, S4A, and S4B). We observed these wide receptive fields along both the horizontal and the vertical axis (Figures 4E and 4F). When we showed both horizontal and vertical Gaussian noise stimuli sequentially while imaging the same layer, vertical and horizontal receptive fields showed the wide spatial extent for the same ROI (Figure S4C). Occasionally, when we mapped axon terminals that were at the edge of the responding brain region, we measured receptive fields with responses of opposite phase consistent with the inhibitory surround (Figure S4B). These surround responses were also extensive in space. Whereas the wide spatial receptive fields were consistent with the extended responses to moving bars (Figures 4A–4C), they were not expected by the columnar restriction of Tm9 arbors in the medulla or the lobula or any known synaptic inputs (Figure 1A) [10, 15]. This suggests that information from multiple columns is converging at the level of Tm9. This convergence is surprising in light of the fact that elementary motion detection formally only requires a local comparison between two neighboring points in space.

The L3-Tm9 Pathway Provides Sustained Signals to Motion Processing

The temporal component of the receptive field that we measured for Tm9 was strongly dominated by the initial lobe of the filter. Similarly, previously measured filters of L3 were monophasic whereas the temporal filters of L1 and L2 were biphasic [7, 13]. These data suggest that the L3-Tm9 pathway displays sustained responses to long-lasting contrast changes, whereas the responses of L2 should be more transient. To test this prediction, we measured the responses of L3 and Tm9 to long light flashes lasting 5 s and compared them to the responses in L2 (Figures 5A and 5B). Both L2 and L3 increased their calcium signal to the offset of light and decreased their calcium signal to light onset, as previously reported in experiments using genetically encoded calcium indicators [7, 13, 27]. Over the course of a 5 s flash, the calcium signals in L2 were transient, decaying back to baseline shortly following light onset or offset (Figure 5B; see also [27]). Conversely, calcium responses in L3 were sustained for both ON and OFF stimuli and did not decrease within the course of 5 s of either light or dark (Figure 5B). Similarly, Tm9 signals decayed only very little during 5 s of darkness and showed completely tonic signals to the ON period. Thus, the L3-Tm9 pathway displays sustained responses to changes in luminance.

Tm9 Is Broadly Required for Responses of Direction-Selective T5 Neurons

Given the unique spatial and temporal properties of Tm9, we next examined its contribution to the direction-selective signals of T5, which receives significant input from Tm9, with only Tm2 having more numerous synapses [8]. To do this, we used two independent binary expression systems to genetically silence Tm9 outputs while expressing GCaMP6f in T4 and T5 neurons (Figures 5C and 5D). T4 and T5 are present in four subtypes with layer-specific projections within the lobula plate. Each subtype displays direction-selective preferences for one of the four cardinal directions of motion [11]. For example, T5 axon terminals in lobula plate layer A preferentially respond to front-to-back motion, whereas axon terminals in layer C respond most strongly to upward motion (Figures 5C and 5D) [11]. To separate the direction-selective responses of each T4 and T5 subtype, we therefore showed individual ON or OFF edges, moving in one of four directions at 20°/s. Strikingly, upon blocking synaptic activity in Tm9, the overall response amplitude of T5 neurons was dramatically reduced for all directions of motion (Figures 5C–5E, 5G, and S5). Whereas the residual responses were still stronger to motion in their preferred direction for some layers, direction selectivity was reduced in all layers (Figures 5F, 5H, and S5). Finally, as expected, silencing Tm9 did not reduce the responses to moving ON edges (Figures 5C and 5D). In summary, blocking Tm9 function dramatically reduced T5 signals, demonstrating that Tm9 is required for elementary motion detection of OFF edges.

Given the unusual temporal kinetics of Tm9, we next wondered whether Tm9 might specifically contribute to the computation of motion at slower speeds. Furthermore, it has been suggested that L3 functions preferentially for the processing of slower motion [23]. We thus sought to test the contribution of Tm9 to the detection of motion of different speeds. To do this, we utilized a motion stimulus that contained moving ON and OFF edges to separate the signals from T4 and T5 yet varied the speed from 10°/s to 150°/s. In control flies, we observed motion responses to OFF edges across all speeds. For example, in axon terminals of layer A, OFF responses were always strongest for edges moving front to back, reflecting the broad speed tuning of T5 (Figure 6A) [11]. Importantly, Tm9 silencing produced a dramatic reduction in T5 responses, as measured using the amplitude of the PD peak. This effect was observed for both slower and faster speeds (Figures 6A–6C). Thus, Tm9 function is critical to OFF edge responses across a broad range of speeds. Taken together, our data argue against a specific role for Tm9 in the processing of only a subset of motion speeds and suggest instead that Tm9 is broadly required for T5 motion responses.

DISCUSSION

Here, we describe a pathway in the *Drosophila* visual system that is required for behavioral responses to OFF edge motion.

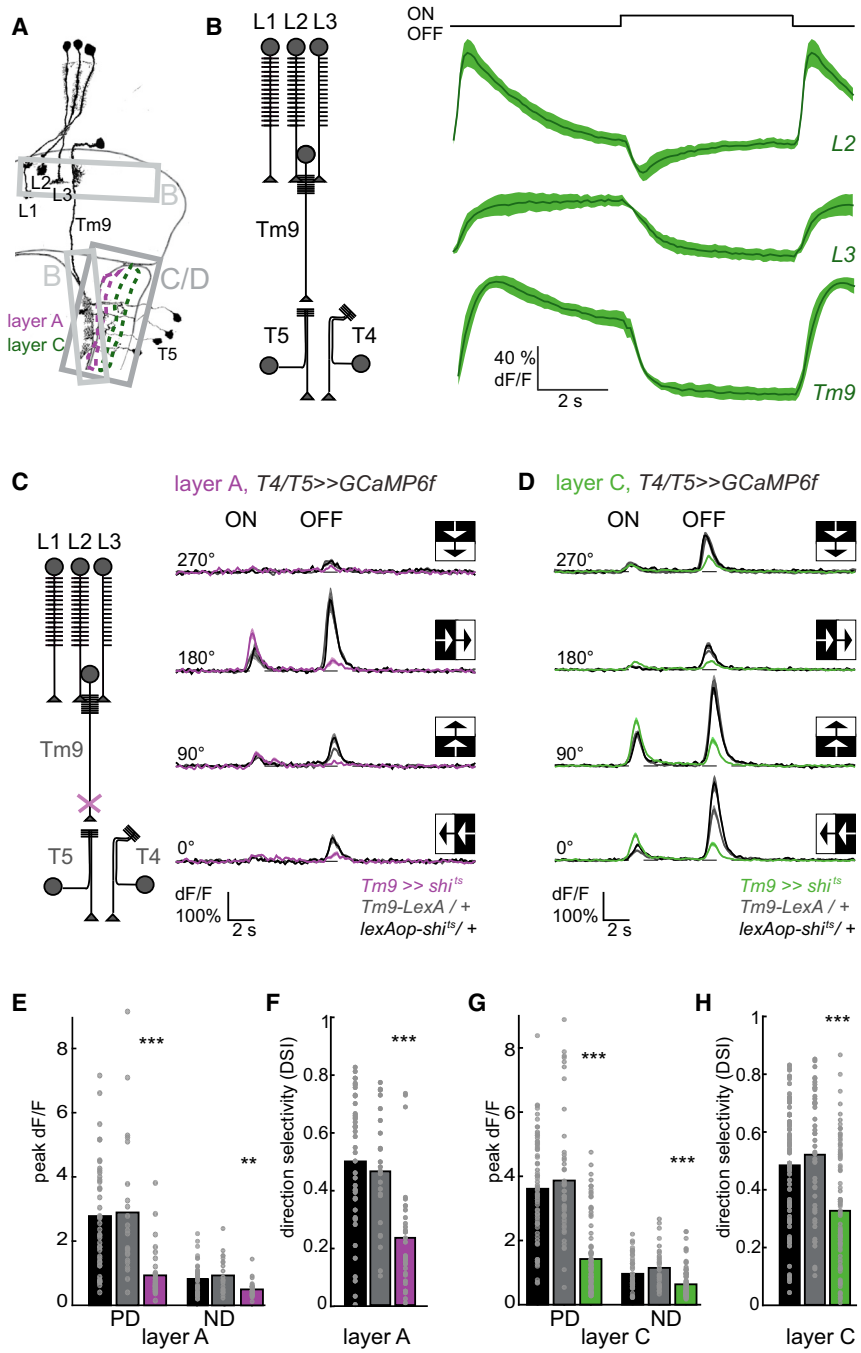

Figure 5. Tm9 Shows Sustained Calcium Signals and Is Required for OFF Edge Responses in T5

(A) Drawing of the fly visual system illustrating lamina neurons L1, L2, and L3; medulla neuron Tm9; and T5 neurons. Gray boxes show regions imaged in (B) and (C) and (D). Adapted from [10].

(B) Average calcium responses (ΔF/F) of L2 axon terminals (top), L3 axon terminals (middle), or Tm9 axon terminals (bottom) to periodic 5-s full-field flashes. Sample sizes are n = 4 flies (71 cells) for L2, n = 5 flies (84 cells) for L3, and n = 4 flies (105 cells) for Tm9.

(C and D) Average calcium responses (ΔF/F) of T4/T5 axon terminals in lobula plate layer A and C to ON and OFF edges moving at 20°/s in four directions while Tm9 neurons were synaptically silenced. Averages were calculated across regions of interest (ROIs) for each layer. All flies were pre-incubated at 37°C for 1 hr prior to imaging.

(E–H) Bar plots showing the peak response to either preferred (PD) or null direction (ND) OFF edge motion or direction selectivity index (DSI) defined as (PD − ND)/(PD + ND) calculated for the response to the moving OFF edge. Sample size for imaging of *T4/T5-Gal4*, *UAS-GCaMP6f* in lobula plate layer A is n = 4 flies (23 ROIs) for the *lexAop-shi^{ts}* control (dark gray), n = 8 (42) for the *Tm9-LexA*/+ control (light gray), and n = 9 (34) for *Tm9-LexA*, *lexAop-shi^{ts}* (magenta) in (C). Sample sizes for imaging of *T4/T5-Gal4*, *UAS-GCaMP6f* in lobula plate layer C are n = 9 flies (70 ROIs) the *lexAop-shi^{ts}* control (dark gray), n = 6 (48) for the *Tm9-LexA*/+ control (light gray), and n = 13 (94) for *Tm9-LexA*, *lexAop-shi^{ts}* layer C (green) in (D). Shading or error bars denote ±1 SEM. **p < 0.01; ***p < 0.001; tested using a Mann-Whitney U-test against both controls.

See also Figure S5.

This pathway links a postsynaptic target of photoreceptors, the lamina neuron L3, to its postsynaptic partner, the medulla neuron Tm9, to the direction-selective neuron T5. Unlike the other known inputs to motion detection, this pathway carries sustained signals that are required for EMD function. Despite its columnar anatomy and the traditional view that inputs to elementary motion detection are local in nature, Tm9 pools inputs across a broad region of space and provides vital contributions to the responses of T5. We also provide the first physiological evidence that demonstrates that L1, the input to the ON motion pathway, also provides input to the OFF motion pathway, corroborating previous behavioral studies [13]. These unexpected properties of peripheral motion-detection circuits challenge current models of elementary motion detection that only consider local inputs and that strictly separate the processing of ON and OFF motion signals.

A combination of anatomical studies, behavioral analysis, and physiological measurements has shed light on the neural circuits that perform motion computation in *Drosophila* (reviewed in [5, 28]). The lamina neurons L1 and L2 were initially identified as the key inputs to motion detection and were characterized extensively [6, 7, 19, 21]. These results were extended by two studies that identified L3 as a third critical input [13, 23]. Here, we use forward genetics to identify Tm9 as a downstream neuron in the L3 pathway, highlighting the power of this approach as an important complement to anatomical predictions. Anatomical and physiological studies suggested that the medulla neurons Mi1 and Tm3 connect L1 to T4 and that Tm1 and Tm2 are important links between L2

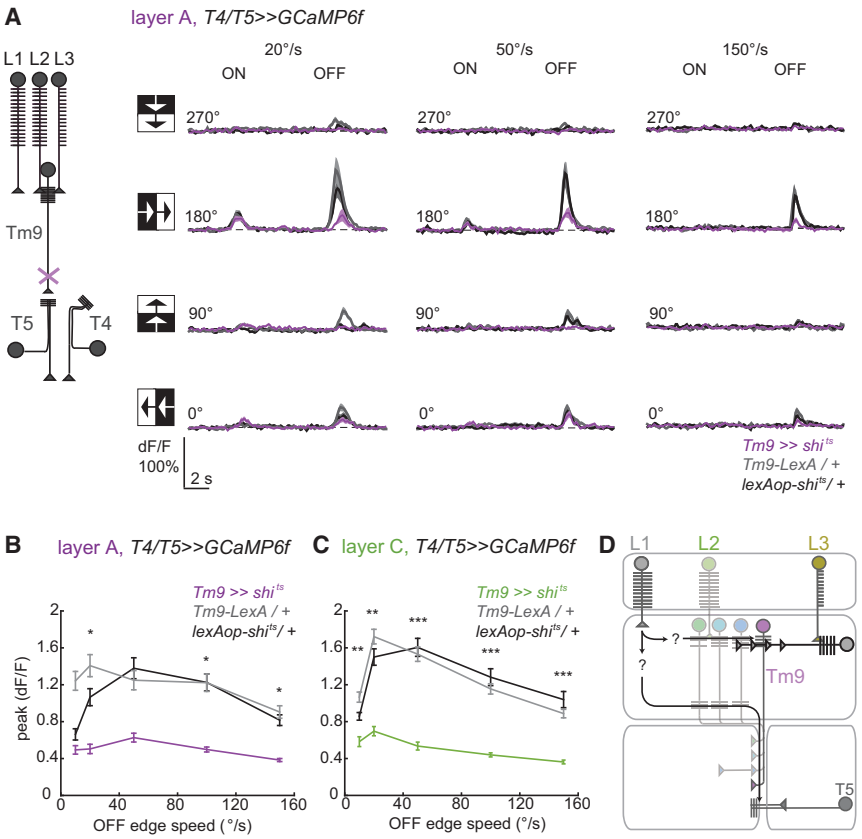

Figure 6. Tm9 Is Required for OFF Edge Responses in T5 Across a Wide Range of Motion Speeds

(A) Average calcium responses (ΔF/F) of T4/T5 axon terminals in lobula plate layer A to ON and OFF edges moving at speeds of 20°/s, 50°/s, and 150°/s in four directions comparing experimental condition where Tm9 neurons were synaptically silenced with two genetic controls.

(B and C) Line graph displays PD peak responses to OFF edges observed across a range of speeds (10°/s– 150°/s). Sample sizes are n = 3 flies (16 ROIs) for the *lexAop-shi^{ts}* control (dark gray), n = 5 flies (23 ROIs) for the *Tm9-LexA*/+ control (light gray), and n = 5 flies (20 cells) for the experimental condition *Tm9-LexA*, *lexAop-shi^{ts}* (magenta) shown in (B). Sample sizes for layer C are n = 6 flies (28 ROIs) for the *lexAop- shi^{ts}* control (dark gray), n = 5 flies (29 ROIs) for the *Tm9-LexA*/+ control (light gray), and n = 5 flies (25 cells) for the experimental condition *Tm9-LexA*, *lexAop-shi^{ts}* (green) shown in (C). *p < 0.05; **p < 0.01; ***p < 0.001; tested using a Mann-Whitney U-test against both controls. Shading or error bars denote ±1 SEM. Averages were calculated across ROIs. All flies were pre-incubated at 37°C for 1 hr prior to imaging.

(D) Schematic of the model of OFF edge motion detection, incorporating results from this study. Tm9 integrates inputs from both L3 and L1. L3 is directly presynaptic to Tm9, but the wide-field responses of Tm9 suggest that these signals must incorporate inputs from several columns potentially via horizontal connections that either directly (as illustrated) or indirectly receive input from L3 and potentially also L1. L1 also has an additional contribution to OFF edge motion detection in a pathway parallel to Tm9.

and T5 [8, 9, 15]. Recent studies have confirmed the contribution of both Mi1 and Tm3 to ON edge motion detection, albeit with varying speed-dependent contributions [29], and a physiological study described a role for Tm2 in OFF motion detection [16]. Our study provides the first physiological and behavioral characterization of a medulla pathway downstream of L3 that is required for elementary motion detection. These data are consistent with previous behavioral studies of L3 and anatomical studies that identified synaptic connections between L3, Tm9, and T5 [8, 13, 15, 23]. Interestingly, whereas our genetic dissection did identify behavioral deficits associated with blocking activity in Tm2, blocking synaptic activity in both L1 and Tm2 did not abolish motion-guided behaviors. Thus, whereas Tm2 likely plays a key role in motion detection, its activity is apparently not strictly required for optomotor responses in walking flies. Given the behavioral salience of motion cues, redundant pathways likely exist that make it harder to identify behavioral phenotypes for neurons that implement core motion computations.

L1 and L3 Inputs Interact at the Level of Tm9

Previous behavioral studies demonstrate that L1 and L3 are functionally redundant for detecting OFF edge motion, such that only silencing both together abolishes behavioral responses to motion [13]. However, how this redundant interaction might manifest in the circuit was unknown. Here, we identify Tm9 as one point of convergence between L1 and L3, as silencing both of these cells together nearly abolishes all Tm9 responses (Figure 6D). Whereas L1 does not appear to provide direct input to Tm9, the second most frequently identified synapses onto Tm9 come from Mi4 [15], which is emerging as one of the circuit elements of the ON pathway (S. Takemura and I. Meinertzhagen, personal communication). It will be interesting to determine the relative contributions of L1 and L3 to the spatiotemporal receptive field structure of Tm9, as one might predict that L1 would preferentially shape the contrast-rectified spatial surround that we observed for Tm9. We note that, in our behavioral experiments, blocking neural activity in L1 also enhances the effect of silencing Tm9 to OFF edge motion. This suggests that additional L1 inputs feed into OFF edge motion detection in a pathway that is parallel to Tm9 (Figure 6D). Taken together, these data suggest that, at least at the level of their inputs, the ON and OFF pathways are not as cleanly separated as is often assumed but rather is in line with previous behavioral data that identified a diversity of lamina inputs for moving OFF edge detection [13]. This relationship between ON and OFF pathways draws interesting analogies to similar observations in the vertebrate retina, where such interactions are used to reconstruct linear responses to contrast via cross-over inhibition [30].

Elementary Motion Detection Uses Sustained, Wide-Field Input

Classic models of elementary motion detection correlate light inputs from adjacent points in visual space to compute motion [3]. Indeed, such local signals are sufficient to evoke direction-selective responses [4, 12, 18]. Recent work has demonstrated that, in *Drosophila*, T5 is the first direction-selective cell in a pathway that processes OFF motion [11]. Direction selectivity can emerge within T5 dendrites through a non-linear interaction between synaptic inputs from nearby medulla columns [12]. By measuring the OFF edge responses of T5 during Tm9 silencing, we tested the contribution of Tm9 to this directional transformation. Our data demonstrate that the synaptic output of Tm9 is vital for OFF pathway signals, as silencing Tm9 dramatically reduces T5 responses. However, our receptive field measurements demonstrate that Tm9 does not provide purely local signals as seen in an HRC. In particular, the size of the Tm9 receptive field gives it the physiological properties of a wide-field neuron. In contrast, electrophysiological measurement of other columnar Tm neurons has revealed receptive field sizes that span approximately 10 degrees of visual space [9]. Thus, circuit mechanisms must exist that provide Tm9 neurons with the unusual ability to pool signals across space. One possibility is a direct coupling of Tm9 neurons via gap junctions. In another scenario, horizontally projecting neurons could connect several Tm9 cells (Figure 6D). Neither gap junctions nor the synaptic connections of these horizontal neurons have been mapped, but tangential cells that span large portions of the medulla represent strong candidates [10, 31].

The physiological properties of Tm9 conflict with the view that T5 receives input from relatively simple circuits that provide local signals that are offset in space and time. One possible resolution could be that, despite its wide receptive field, Tm9 may still provide local signals. Consistent with this, Tm9 responds strongly to stimuli that only partially fill its receptive field, such as moving bar stimuli. Alternatively, the function of Tm9 might indeed fully utilize its wide-field properties. In this view, instead of being part of a circuit that compares local signals, Tm9 may provide a gating mechanism for direction-selective T5 neurons. In particular, additional drive from wide-field inputs may help motion-detecting circuits respond well to large moving objects that are highly behaviorally relevant and may also reduce noise from fast local contrast changes. Consistent with this notion, T5 neurons display stronger responses to large moving edges compared to spatially localized moving bars [12].

The temporal response properties of Tm9 are substantially more sustained than those previously characterized in the other OFF motion pathway elements Tm1 and Tm2, which have relatively transient responses [9]. Interestingly, such tonic signals have been inferred both physiologically and behaviorally using apparent motion stimuli that demonstrate directional interactions over timescales of up to 10 s [7, 32, 33]. These data argue that the fly EMD utilizes information about contrast changes over a much-longer timescale than the transient response properties of Tm1 and Tm2 would predict. L3 and Tm9 may provide neural substrates for such tonic signals within the OFF motion-detecting pathway, and our data demonstrate that these elements are vital for OFF edge motion signals within T5. Finally, it is interesting that both tonic and wide-field signals appear in the same pathway. Utilizing sustained wide-field inputs could be useful under certain stimulus regimes when such properties could make the motion circuit more robust, even if this entails a concomitant loss in spatial and temporal precision.

Given the incomplete segregation of ON and OFF motion pathways that we observe, combined with the non-canonical receptive field properties of Tm9, we infer that the neural implementation of elementary motion-detecting pathways is more complex and diverse than previously proposed. It will be interesting to dissect the underlying circuit architecture and to understand how this computational richness shapes motion-guided behaviors.

EXPERIMENTAL PROCEDURES

Fly Stocks

Driver Lines Used

The InSITE Gal4 lines used in this study were *0682-Gal4* (*PBac{IT.GAL4}0682*) and *0137-Gal4* (*PBac{IT.GAL4}0137*). Genetic InSITE swaps were performed as described in [34]. Gal4 was replaced by the genetic donors {*ID.p65AD*}*P14.1*, {*ID.VP16AD*}*33.1*, and {*ID.IVS-GAL80-WPRE*} [34, 35] to generate the InSITE swaps *PBac{IS.IVS-GAL80-WPRE}0137* (*0137 -Gal80*), *PBac{IS.p65-AD}0137* (*0137-p65AD*), and *PBac{IT.GAL4}0682* to *PBac{IS.VP16-AD}0682* (*0682-VP16AD*). Genetic intersections were done using *cha-Gal4DBD* and *cha-Gal80*. Driver lines used for genetic silencing of lamina neurons were $L1^{c202a}$-*Gal4*, $L2^{21Dhh}$-*Gal4*, and $L3^{0595}$-*Gal4* [13, 19]. Tm9-LexA is $Tm9^{R24C08}$-*LexA::VP16AD*^{attP40} as described in [24]. Additionally, $L3^{MH56}$-*Gal4* [36] and $T4/T5^{R42F06}$-*Gal4* ^{attP2} [11] were used for in vivo calcium imaging.

Effector Lines Used

UAS-shi^{ts}, *UAS-mCD8::GFP*, *UAS-EGFP*, *UAS-Flp*, *UAS-GCaMP6f*^{attP40}, *lexAop-mCD8::GFP*^{attP8}, *lexAop-GCaMP6F*^{attP5}, *UAS-mCD8::RFP*^{attP18} (BDSC), and *UAS > CD2,y*$^{+}$ *> mCD8:: GFP* were used [22]. *lexAop-shi*$^{ts\text{-}attP2}$ was generated in this study (see Supplemental Experimental Procedures).

Behavioral Experiments

Behavioral experiments with tethered flies walking on an air-suspended ball were done as described in [7], with modifications as described in [13]. In brief, fly turning was measured while flies were shown different rotational stimuli (rotating square wave gratings, rotating ON or OFF edges, or opposing edges). Female flies of all genotypes were tested at the restrictive temperature for *shi*^{ts} activity, at 34°C.

Calcium Imaging

In vivo calcium imaging experiments were performed on a Leica SP5 two-photon microscope or a Zeiss 7MP (Figure 3), using 920-nm light from a Chameleon Vision II laser. GCaMP6f was expressed either in L2, L3, Tm9, or T4/T5 neurons using the Gal4 and LexA drivers described above. Simultaneous silencing of synaptic transmission was performed using *UAS-shibire*^{ts} or *lexAop-shibire*^{ts} (generated in this study) upon pre-incubation in a 37°C water bath for 1 hr, followed by a maximum experimental time of 30 min.

See Supplemental Experimental Procedures for detailed methods.

SUPPLEMENTAL INFORMATION

Supplemental Information includes five figures and Supplemental Experimental Procedures and can be found with this article online at http://dx.doi.org/10.1016/j.cub.2015.11.018.

AUTHOR CONTRIBUTIONS

M.S. and T.R.C. designed and planned the study. M.S., Y.E.F., J.C.S.L., K.S., M.D.K., and D.M.G. performed experiments. J.C.S.L., Y.E.F., K.S., and M.S. analyzed the data. Y.E.F., T.R.C., and M.S. wrote the manuscript.

ACKNOWLEDGMENTS

We thank Christine Gündner for excellent technical support, André Fiala for generous access to a 2P microscope, Arezoo Pooresmaeili for comments on the manuscript, and the BDSC and Nirao Shah for fly stocks. This work was supported by the Deutsche Forschungsgemeinschaft (DFG) through an Emmy Noether grant and CRC 889—project C8 to M.S. and R01EY022638 to T.R.C. J.C.S.L. acknowledges Stanford MSTP, Stanford Bio-X, and Neuroadventures, and Y.E.F. acknowledges an NSF Fellowship.

Received: July 22, 2015
Revised: October 5, 2015
Accepted: November 5, 2015
Published: December 3, 2015

REFERENCES

1. Borst, A., and Euler, T. (2011). Seeing things in motion: models, circuits, and mechanisms. Neuron *71*, 974–994.
2. Clifford, C.W.G., and Ibbotson, M.R. (2002). Fundamental mechanisms of visual motion detection: models, cells and functions. Prog. Neurobiol. *68*, 409–437.
3. Hassenstein, B., and Reichardt, W. (2014). Systemtheoretische analyse der zeit-, reihenfolgen- und vorzeichenauswertung bei der bewegungsperzeption des rüsselkäfers *Chlorophanus*. Zeitschrift für Naturforschung *11*, 513–524.
4. Franceschini, N., Pichon, J.M., and Blanes, C. (1992). From insect vision to robot vision. Philos. Trans. R. Soc. Lond. B *337*, 283–294.
5. Silies, M., Gohl, D.M., and Clandinin, T.R. (2014). Motion-detecting circuits in flies: coming into view. Annu. Rev. Neurosci. *37*, 307–327.
6. Joesch, M., Schnell, B., Raghu, S.V., Reiff, D.F., and Borst, A. (2010). ON and OFF pathways in Drosophila motion vision. Nature *468*, 300–304.
7. Clark, D.A., Bursztyn, L., Horowitz, M.A., Schnitzer, M.J., and Clandinin, T.R. (2011). Defining the computational structure of the motion detector in Drosophila. Neuron *70*, 1165–1177.
8. Shinomiya, K., Karuppudurai, T., Lin, T.-Y., Lu, Z., Lee, C.-H., and Meinertzhagen, I.A. (2014). Candidate neural substrates for off-edge motion detection in Drosophila. Curr. Biol. *24*, 1062–1070.
9. Behnia, R., Clark, D.A., Carter, A.G., Clandinin, T.R., and Desplan, C. (2014). Processing properties of ON and OFF pathways for Drosophila motion detection. Nature *512*, 427–430.
10. Fischbach, K.-F., and Dittrich, A.P.M. (1989). The optic lobe of *Drosophila melanogaster*. I. A Golgi analysis of wild-type structure. Cell Tissue Res. *258*, 441–475.
11. Maisak, M.S., Haag, J., Ammer, G., Serbe, E., Meier, M., Leonhardt, A., Schilling, T., Bahl, A., Rubin, G.M., Nern, A., et al. (2013). A directional tuning map of Drosophila elementary motion detectors. Nature *500*, 212–216.
12. Fisher, Y.E., Silies, M., and Clandinin, T.R. (2015). Orientation selectivity sharpens motion detection in Drosophila. Neuron *88*, 390–402.
13. Silies, M., Gohl, D.M., Fisher, Y.E., Freifeld, L., Clark, D.A., and Clandinin, T.R. (2013). Modular use of peripheral input channels tunes motion-detecting circuitry. Neuron *79*, 111–127.
14. Schnell, B., Raghu, S.V., Nern, A., and Borst, A. (2012). Columnar cells necessary for motion responses of wide-field visual interneurons in Drosophila. J. Comp. Physiol. A Neuroethol. Sens. Neural Behav. Physiol. *198*, 389–395.
15. Takemura, S.-Y., Bharioke, A., Lu, Z., Nern, A., Vitaladevuni, S., Rivlin, P.K., Katz, W.T., Olbris, D.J., Plaza, S.M., Winston, P., et al. (2013). A visual motion detection circuit suggested by Drosophila connectomics. Nature *500*, 175–181.
16. Meier, M., Serbe, E., Maisak, M.S., Haag, J., Dickson, B.J., and Borst, A. (2014). Neural circuit components of the Drosophila OFF motion vision pathway. Curr. Biol. *24*, 385–392.
17. Morante, J., and Desplan, C. (2008). The color-vision circuit in the medulla of Drosophila. Curr. Biol. *18*, 553–565.
18. Buchner, E. (1976). Elementary movement detectors in an insect visual system. Biol. Cybern. *24*, 85–101.
19. Rister, J., Pauls, D., Schnell, B., Ting, C.-Y., Lee, C.-H., Sinakevitch, I., Morante, J., Strausfeld, N.J., Ito, K., and Heisenberg, M. (2007). Dissection of the peripheral motion channel in the visual system of Drosophila melanogaster. Neuron *56*, 155–170.
20. Kitamoto, T. (2001). Conditional modification of behavior in Drosophila by targeted expression of a temperature-sensitive shibire allele in defined neurons. J. Neurobiol. *47*, 81–92.
21. Katsov, A.Y., and Clandinin, T.R. (2008). Motion processing streams in Drosophila are behaviorally specialized. Neuron *59*, 322–335.
22. Wong, A.M., Wang, J.W., and Axel, R. (2002). Spatial representation of the glomerular map in the Drosophila protocerebrum. Cell *109*, 229–241.
23. Tuthill, J.C., Nern, A., Holtz, S.L., Rubin, G.M., and Reiser, M.B. (2013). Contributions of the 12 neuron classes in the fly lamina to motion vision. Neuron *79*, 128–140.
24. Fan, P., Manoli, D.S., Ahmed, O.M., Chen, Y., Agarwal, N., Kwong, S., Cai, A.G., Neitz, J., Renslo, A., Baker, B.S., and Shah, N.M. (2013). Genetic and neural mechanisms that inhibit Drosophila from mating with other species. Cell *154*, 89–102.
25. Freifeld, L., Clark, D.A., Schnitzer, M.J., Horowitz, M.A., and Clandinin, T.R. (2013). GABAergic lateral interactions tune the early stages of visual processing in Drosophila. Neuron *78*, 1075–1089.
26. Gao, S., Takemura, S.-Y., Ting, C.-Y., Huang, S., Lu, Z., Luan, H., Rister, J., Thum, A.S., Yang, M., Hong, S.-T., et al. (2008). The neural substrate of spectral preference in Drosophila. Neuron *60*, 328–342.
27. Strother, J.A., Nern, A., and Reiser, M.B. (2014). Direct observation of ON and OFF pathways in the Drosophila visual system. Curr. Biol. *24*, 976–983.
28. Borst, A. (2014). In search of the Holy Grail of fly motion vision. Eur. J. Neurosci. *40*, 3285–3293.
29. Ammer, G., Leonhardt, A., Bahl, A., Dickson, B.J., and Borst, A. (2015). Functional Specialization of Neural Input Elements to the Drosophila ON Motion Detector. Curr. Biol. *25*, 2247–2253.
30. Werblin, F.S. (2010). Six different roles for crossover inhibition in the retina: correcting the nonlinearities of synaptic transmission. Vis. Neurosci. *27*, 1–8.
31. Nern, A., Pfeiffer, B.D., and Rubin, G.M. (2015). Optimized tools for multicolor stochastic labeling reveal diverse stereotyped cell arrangements in the fly visual system. Proc. Natl. Acad. Sci. USA *112*, E2967–E2976.
32. Egelhaaf, M., and Borst, A. (1992). Are there separate ON and OFF channels in fly motion vision? Vis. Neurosci. *8*, 151–164.
33. Eichner, H., Joesch, M., Schnell, B., Reiff, D.F., and Borst, A. (2011). Internal structure of the fly elementary motion detector. Neuron *70*, 1155–1164.
34. Gohl, D.M., Silies, M.A., Gao, X.J., Bhalerao, S., Luongo, F.J., Lin, C.-C., Potter, C.J., and Clandinin, T.R. (2011). A versatile in vivo system for directed dissection of gene expression patterns. Nat. Methods *8*, 231–237.
35. Gao, X.J., Potter, C.J., Gohl, D.M., Silies, M., Katsov, A.Y., Clandinin, T.R., and Luo, L. (2013). Specific kinematics and motor-related neurons for aversive chemotaxis in Drosophila. Curr. Biol. *23*, 1163–1172.
36. Timofeev, K., Joly, W., Hadjieconomou, D., and Salecker, I. (2012). Localized netrins act as positional cues to control layer-specific targeting of photoreceptor axons in Drosophila. Neuron *75*, 80–93.